

MIT Open Access Articles

Genome-wide CRISPR Screen in a Mouse Model of Tumor Growth and Metastasis

The MIT Faculty has made this article openly available. **Please share** how this access benefits you. Your story matters.

Citation: Chen, Sidi et al. "Genome-Wide CRISPR Screen in a Mouse Model of Tumor Growth and Metastasis." *Cell* 160, 6 (March 2015): 1246–1260 © 2015 Elsevier Inc

As Published: <http://dx.doi.org/10.1016/j.cell.2015.02.038>

Publisher: Elsevier

Persistent URL: <http://hdl.handle.net/1721.1/111184>

Version: Author's final manuscript: final author's manuscript post peer review, without publisher's formatting or copy editing

Terms of use: Creative Commons Attribution-NonCommercial-NoDerivs License





Published in final edited form as:

Cell. 2015 March 12; 160(6): 1246–1260. doi:10.1016/j.cell.2015.02.038.

Genome-wide CRISPR screen in a mouse model of tumor growth and metastasis

Sidi Chen^{1,2,3,*}, Neville E. Sanjana^{3,4,5,6,7,*}, Kaijie Zheng^{3,4}, Ophir Shalem^{3,4}, Kyunghoon Lee⁸, Xi Shi^{3,4}, David A. Scott^{3,4}, Jun Song⁸, Jen Q. Pan^{3,4}, Ralph Weissleder^{8,9}, Hakho Lee⁸, Feng Zhang^{3,4,5,6,7,#}, and Phillip A. Sharp^{1,2,#}

¹David H. Koch Institute for Integrative Cancer Research, Cambridge, MA 02139, USA

²Department of Biology, Cambridge, MA 02139, USA

³Broad Institute of MIT and Harvard, Cambridge, MA 02142, USA

⁴Stanley Center for Psychiatric Research, Cambridge, MA 02142, USA

⁵McGovern Institute for Brain Research, Massachusetts Institute of Technology, Cambridge, MA 02139, USA

⁶Department of Brain and Cognitive Sciences, Massachusetts Institute of Technology, Cambridge, MA 02139, USA

⁷Department of Biological Engineering, Massachusetts Institute of Technology, Cambridge, MA 02139, USA

⁸Center for Systems Biology, Massachusetts General Hospital, Boston, MA 02114, USA

⁹Department of Systems Biology, Harvard Medical School, Boston, MA 02115, USA

Summary

Genetic screens are powerful tools for identifying genes responsible for diverse phenotypes. Here we describe a genome-wide CRISPR-Cas9-mediated loss-of-function screen in tumor growth and metastasis. We mutagenized a non-metastatic mouse cancer cell line using a genome-scale library with 67,405 single guide RNAs (sgRNAs). The mutant cell pool rapidly generates metastases when transplanted into immunocompromised mice. Enriched sgRNAs in lung metastases and late stage primary tumors were found to target a small set of genes, suggesting specific loss-of-

© 2015 Published by Elsevier Inc.

#Corresponding authors: PAS (sharppa@mit.edu), FZ (zhang@broadinstitute.org).

*Co-first authors

Accession

Genomic sequencing data are deposited in NCBI SRA under accession PRJNA273894.

Author contributions

SC, NS, OS, FZ, PAS conceived and designed the study. SC, NS, KZ performed all screening and validation experiments. SC, NS, OS, DAS analyzed the data. KL, JS, RW, HL designed the CTC chip and performed CTC analysis. XS, JP performed western blots. SC, NS, FZ, PAS wrote the paper with the input from all other authors. PAS and FZ supervised the work.

Publisher's Disclaimer: This is a PDF file of an unedited manuscript that has been accepted for publication. As a service to our customers we are providing this early version of the manuscript. The manuscript will undergo copyediting, typesetting, and review of the resulting proof before it is published in its final citable form. Please note that during the production process errors may be discovered which could affect the content, and all legal disclaimers that apply to the journal pertain.

function mutations drive tumor growth and metastasis. Individual sgRNAs and a small pool of 624 sgRNAs targeting the top scoring genes from the primary screen dramatically accelerate metastasis. In all of these experiments, the effect of mutations on primary tumor growth positively correlates with the development of metastases. Our study demonstrates Cas9-based screening as a robust method to systematically assay gene phenotypes in cancer evolution *in vivo*.

Keywords

CRISPR/Cas9; metastasis; genome-wide screen; cancer evolution

Introduction

Cancer genomes have complex landscapes of mutations and diverse types of genetic aberrations (Lawrence et al., 2013; Weinberg, 2007). A major challenge in understanding the cancer genome is to disentangle alterations that are driving the processes of tumor evolution from passenger mutations (Garraway and Lander, 2013). Primary tumor growth and metastasis are distinct yet linked processes in the progression of solid tumors (Nguyen et al., 2009; Valastyan and Weinberg, 2011; Vanharanta and Massague, 2013). It has been observed in the clinic that the probability of detecting metastases in a patient positively correlates with the size of a primary tumor (Heimann and Hellman, 1998). Several possible explanations have been suggested: metastatic properties may only be acquired in late-stage tumors; larger tumors proportionally seed more cells into circulation that eventually migrate to other sites; or that cells with a strong ability to proliferate also have enhanced ability to metastasize (Weinberg, 2007). In early studies using random insertional mutagenesis, it was observed that metastatic cell subpopulations overgrow to complete dominance in the primary tumor, suggesting progressive selection at both sites (Korczak et al., 1988; Waghorne et al., 1988).

Genetic screens are powerful tools for assaying phenotypes and identifying causal genes in various hallmarks of cancer progression (Hanahan and Weinberg, 2011). RNA interference (RNAi), or overexpression of open reading frames (ORFs), have been utilized for screening cancer genes in several models of oncogenesis in mice (Schramek et al., 2014; Shao et al., 2014; Zender et al., 2008). Recently, the Cas9 nuclease (Barrangou et al., 2007; Bolotin et al., 2005; Chylinski et al., 2013; Chylinski et al., 2014; Deltcheva et al., 2011; Garneau et al., 2010; Gasiunas et al., 2012; Jinek et al., 2012; Sapranaukas et al., 2011) from the microbial type II CRISPR (Clustered Regularly Interspaced Short Palindromic Repeats) system has been harnessed to facilitate loss-of-function mutations in eukaryotic cells (Cong et al., 2013; Mali et al., 2013). When the Cas9 nuclease is targeted to specific locations in the genome, DNA cleavage results in double-stranded breaks (DSBs), which are repaired via non-homologous end-joining (NHEJ) (Rouet et al., 1994). NHEJ repair results in insertion or deletion (indel) mutations that can cause loss-of-function if the DSB occurs in a coding exon. The Cas9 nuclease can be guided to its DNA target by a single guide RNA (sgRNA) (Jinek et al., 2012), a synthetic fusion between the CRISPR RNA (crRNA) and trans-activating crRNA (tracrRNA) (Deltcheva et al., 2011). In cells, Cas9-mediated gene disruption requires the full-length tracrRNA (Cong et al., 2013; Mali et al., 2013), in which

secondary structures at the 3' end of tracrRNA are critical for Cas9-mediated genome modification (Cong et al., 2013; Hsu et al., 2013).

Screens utilizing Cas9 have identified genes that are essential for cell survival and genes involved in drug resistance in various cell lines (Koike-Yusa et al., 2014; Shalem et al., 2014; Wang et al., 2014; Zhou et al., 2014). *In vivo* pooled screens are challenging due to many factors, such as the complexity of the library, limitations of virus delivery and/or cell transplantation, uniformity of viral transduction at a low multiplicity of infection (MOI), and the complex dynamics and interactions of cells in animals. In this study, we report a genome-wide Cas9 knockout screen in a mouse model of tumor evolution. This screen provides a systematic phenotypic measurement of loss-of-function mutations in primary tumor growth and metastasis.

Results

CRISPR/Cas9 library-mediated mutagenesis promotes metastasis

We derived and cloned a cell line (Chen et al., 2014) from a mouse non-small cell lung cancer (NSCLC) (Kumar et al., 2009). This cell line possesses an oncogenic *Kras* in conjunction with homozygous *p53* and heterozygous *Dicer1* loss of function (*Kras*^{G12D}/₊;*p53*^{-/-};*Dicer1*^{+/-}, denoted KPD), and is capable of inducing tumors when transplanted into immunocompromised mice (Chen et al., 2014; Kumar et al., 2009). We transduced this cell line with a lentivirus carrying a Cas9 transgene fused to a green fluorescent protein (GFP) and generated clonal cell lines (Cas9-GFP KPD) (Experimental Procedures) (Figure S1 A–B). A clonal Cas9-GFP KPD cell line (clone 5) was selected to provide genetic and cellular homogeneity for subsequent screens.

We utilized a pooled genome-wide mouse sgRNA library (termed mouse Genome-scale CRISPR knockout library A, or mGeCKOa) containing 67,405 sgRNAs targeting 20,611 protein-coding genes and 1,175 microRNA precursors in the mouse genome (Sanjana et al., 2014). The library also contains 1,000 control sgRNAs (termed non-targeting sgRNAs) designed to have minimal homology to sequences in the mouse genome (Sanjana et al., 2014; Shalem et al., 2014). We transduced the Cas9-GFP KPD cell line with mGeCKOa with three independent infection replicates and each replicate with greater than 400x library coverage (cells per lentiviral CRISPR construct) (Figure 1A) (Experimental Procedures).

After *in vitro* culture for 1 week, we subcutaneously transplanted 3×10^7 cells into the flanks of immunocompromised *Nu/Nu* mice (Figure 1A). We transplanted the cells from each infection replicate into 4 mice, using 1 mouse for early tumor sequencing and 3 mice for sequencing of late stage primary tumor and metastases (Figure 1A). Both mGeCKOa transduced and untransduced Cas9-GFP KPD cells formed tumors at the injection site (Figure 1B). Like most subcutaneously transplanted tumors, these tumors were poorly differentiated. The primary tumors induced by mGeCKOa transduced cells grew slightly faster than tumors from the untransduced cells at an early stage (Figure 1C) (two weeks post-transplantation) (paired two-tailed *t*-test, $p = 0.05$), but at late stages all tumors were similar in size (paired two-tailed *t*-test, $p = 0.18$ for data at four weeks, and $p = 0.6$ for data at six weeks) (Figure 1C).

At 6 weeks post-transplantation, we imaged the mice using micro-computed tomography (μ CT), and found tumors in the lungs of the mice transplanted with mGeCKOa-transduced Cas9-GFP KPD cells (mGeCKOa mice), but not in the mice transplanted with untransduced Cas9-GFP KPD cells (control mice) (Figure 1D, Figure S1 C). Mice were sacrificed and examined for metastases in various organs. Under a fluorescent stereoscope at 6x magnification, metastases were visually detected in the lung in 90% (8/9) of the mGeCKOa mice (Figure S1 D). The mGeCKOa mice on average had 80% of their lung lobes positive for metastases (Figure 1E). In contrast, none (0/3) of the control mice developed detectable metastases in the lung (Figure 1E). At this time, metastases were not detected in the liver, kidney or spleen in either group (Figure 1F). These data indicated that mGeCKOa library transduction enhanced the ability of the Cas9-GFP KPD cells to form metastases in the lung.

Dynamic evolution of sgRNA library representation during tumor growth and metastasis

To investigate the sgRNA representation through different stages of tumor evolution and to identify genes where loss-of-function confers a proliferative or metastatic phenotype, we used deep sequencing to read out the sgRNA representation. At six weeks post transplantation, we sequenced the late stage primary tumor and three random lobes from the lung of each of the nine mGeCKOa mice (Figure 1A) (Experimental Procedures). In parallel, we also sequenced the mGeCKOa input plasmid library, the pre-transplantation mGeCKOa transduced Cas9-GFP KPD cells (cultured *in vitro* for 7 days after transduction), as well as early stage primary tumors (two weeks post transplantation, one mouse from each infection replicate). In the cell samples, the sgRNA representations showed high concordance between technical replicates (correlation, $\rho = 0.95$ on average, $n = 3$) and biological infection replicates (correlation, $\rho = 0.84$ on average, $n = 3$) (Figure 2A, Figure S2 A, B, E). The sgRNA representation of cell samples highly correlates with the plasmid representation (correlation, $\rho = 0.93$ on average, $n = 3$) (Figure 2A, Figure S2 C, E). Furthermore, different sgRNAs that target the same gene are correlated in terms of rank change (correlation, $\rho = 0.49$ on average, $n = 3$) (Figure S2 D). Using Gene Set Enrichment Analysis, we found that the sgRNAs with significantly decreased abundance in cells compared to plasmid are enriched for genes involved in fundamental cellular processes, such as ribosomal proteins, translation factors, RNA splicing factors and RNA processing factors, indicating selection against the loss of these genes after one week in culture (Figure S2 F).

To investigate the sgRNA library dynamics in different sample types (plasmid, pre-transplantation cells, early primary tumor, late primary tumor, and lung metastases), we compared the overall distributions of sgRNAs from all samples sequenced. Cell samples tightly clustered with each other and the plasmid, forming a cell-plasmid clade (Figure 2A, Figure S2 E). Early primary tumor samples also clustered with each other and then with the cell-plasmid clade, whereas late tumors and lung metastases clustered together in a distinct group (Figure 2A, Figure S2 E). The overlap of detected sgRNAs between different pre-transplantation infection replicates is over 95% (Figure S3 A). The detected sgRNAs in the three infection replicates of early tumor samples overlap 63 – 76% with each other (Figure S3 B). Early primary tumors retained less than half (32 – 49%) of the sgRNAs found in the transplanted cell populations (Figure 2B–C, Figure S3 C–D). Compared to the cell

populations, sgRNAs whose targets are genes involved in fundamental cellular processes are further depleted in early tumors (Table S1).

Interestingly, only a small fraction of sgRNAs (less than 4% of all sgRNAs, or less than 8% of sgRNAs in the early primary tumor of the corresponding replicate) were detected in the late stage primary tumor samples (Figure 2B–C, Figure S3 C–D). The sgRNA diversity (i.e. number of different sgRNAs detected) further decreased in samples from lung metastases (Figure 2B–C, Figure S3 C–D). The lung samples retained 0.4% of all sgRNAs in the mGeCKOa library, or 1.1% of sgRNAs found in the early primary tumor of the corresponding replicate, with a subset of highly enriched sgRNAs (Figure 2B–C, Figure S3 C–D). The global patterns of sgRNA distributions in different sample types are distinct, as is evident in the strong shifts in the respective cumulative distribution functions (Kolmogorov-Smirnov (KS) test, $p < 10^{-15}$ for all pairwise comparisons) (Figure 2D).

Enriched sgRNAs in primary tumors

Late primary tumors retain few sgRNAs (on average 813 ± 264 sgRNAs, $n = 9$ mice), with even fewer at high frequencies (4 ± 1 sgRNAs with $> 5\%$ of total reads) in each mouse (Figure 2B–C, Figure S2 C–D, Figure 3A, Figure S4 H). We used three methods to identify enriched sgRNAs in the late primary tumor: (1) sgRNAs above a certain threshold, (2) top ranked sgRNAs in the tumor of each mouse, and (3) using the false discovery rate (FDR), i.e. sgRNAs enriched compared to the distribution of the 1,000 non-targeting sgRNAs. All three methods generated similar results (Figure S4 A). Taking the results from (3) as an example, a total of 935 sgRNAs (targeting 909 genes) are enriched over the non-targeting controls (FDR cutoff = 0.2%) in the late primary tumor of one or more mice (Figure 3B–C). These sgRNAs are targeting genes highly enriched in apoptosis pathways (Table S2), with many of them being pro-apoptotic, such as *BH3 interacting-domain death agonist (Bid)*, *Phosphatase and Tensin Homolog (Pten)*, *Cyclin-dependent kinase inhibitor 2a (Cdkn2a)*, and *O-6-Methylguanine-DNA Methyltransferase (Mgmt)*, suggesting strong selection for mutations that inactivate apoptosis in primary tumor cells.

We identified 24 candidate genes that were targeted by two or more independent sgRNAs enriched in late primary tumors (Figure 3B–C). These genes were found to be mutated in patients in many previously reported cancer sequencing studies curated by cBioPortal (Cerami et al., 2012; Gao et al., 2013) (Figure S5 A). For example, in somatic mutations identified by The Cancer Genome Atlas (TCGA) for non-small cell lung cancer (NSCLC), including adenocarcinoma (LUAD) (TCGA-Network, 2014) and lung squamous cell carcinoma (LUSC) (TCGA-Network, 2012), 36% (107/407) of the patients have one or more of these 24 genes mutated (Figure S5 B–C). Several candidates were well-known tumor suppressors, such as *Pten*, *Cyclin-dependent kinase inhibitor 2b (Cdkn2b)*, *Neurofibromin 2 (Nf2, Merlin)*, *Alpha-type platelet-derived growth factor receptor (Pdgfra)*, and *Integrin alpha X (Itgax)*.

Enriched sgRNAs in metastases

We also sequenced the sgRNA distributions from three lung lobes for each mouse transplanted with mGeCKOa-transduced Cas9-GFP KPD cells. In each lobe, the sgRNA

representation is dominated by one or a few sgRNAs (Figure 4A, Figure S3 D, Figure S4 I). In each mouse, the lung sgRNA representation (average of normalized sgRNA representations from three lobes) is also dominated by a small number of sgRNAs (on average, 3.4 ± 0.4 sgRNAs with $> 5\%$ of total reads) (Figure 4B), suggesting that metastases were seeded by a small set of cells, which grew to dominance over this time scale. Non-targeting sgRNAs were occasionally detected in the metastases, but never observed at high frequency ($< 0.1\%$ of total reads in any lobe; Figure 2C, Figure 4A–B, Figure S4 I). These observations are consistent with our finding that untransduced tumors are not metastatic (Figure 1E), suggesting specific sgRNA-mediated mutations led to metastasis.

The sgRNA representations in the lung metastases are similar to those in the late stage primary tumors in several ways. First, the detected sgRNAs in lung samples significantly overlap with those in late tumor samples (Chi-square test, $p < 10^{-15}$) (Figure S3 E). Second, the number of sgRNAs detected in lung samples correlates, albeit weakly, with the number of sgRNAs detected in late primary tumor samples ($\rho = 0.42$, F-test, $p = 0.097$) (Figure S3 F). Third, the abundance (number of reads) of sgRNAs in the lung positively correlates with that in the late primary tumors of the same mouse (correlation, $\rho = 0.18$ on average, F-test, $p < 0.01$, $n = 9$) (Figure S3 G). Fourth, in most mice (8/9), the lung metastasis enriched sgRNAs also occupy a large fraction of reads in the late primary tumor of the same mouse (Figure 4C, left panel), significantly larger than a random sampling of the same number of sgRNAs from the mGeCKOa library (Figure 4C, right panel). These data indicate that mutants with preferential ability to proliferate in late primary tumors are more likely to dominate the metastases.

The three methods (threshold, rank, or FDR) of finding enriched sgRNAs in the lung metastases yield similar results (Figure S4 B). Using the non-targeting sgRNA distribution to set a FDR-based cutoff for enrichment, the enriched sgRNAs in different lobes of the same mouse overlap with each other by $62\% \pm 5\%$ (Chi-square test, $p < 10^{-15}$) (Figure S4 C), while different mice show greater variability while still overlapping significantly ($29\% \pm 3\%$ Chi-square test, $p < 10^{-15}$) (Figure S4 D). The overlap between sgRNAs in different biological / infection replicate experiments when pooling enriched sgRNAs from all mice in the same replicate is 54% (Chi-square test, $p < 10^{-15}$) (Figure S4 E), suggesting pooling sgRNAs from mice in the same experiment facilitates the identification of shared hits. These data suggest that the three independent experiments reproducibly captured a common set of hits, and provides a picture for *in vivo* experimental variation between different lobes, different animals and different infection replicates.

We found 147 sgRNAs enriched in more than one lobe, and 105 sgRNAs enriched in the lung of more than one mouse (Figure 4D–E). These include sgRNAs targeting *Nf2*, *Pten*, *Tripartite motif-containing protein 72 (Trim72)*, *Fibrinogen Alpha Chain (Fga)*, *Bid*, *Cyclin-dependent kinase inhibitor 2a (Cdkn2a)*, *Zinc Finger FYVE Domain Containing 28 (Zfyve28)*, *Reproductive homeobox 13 (Rhox13)*, *BRISC* and *BRCA1 A complex member 1 (Babam1)*, as well as microRNA genes *miR-152* and *miR-345*. Intriguingly, a few sgRNAs targeting the Pol II subunits and olfactory receptor are also enriched in the lung, possibly due to off-target effects or unknown roles of these genes. For most sgRNAs detected in lung metastases, the relative abundance in metastases is lower than that in the late primary tumor

of the same mouse, with a metastasis-primary ratio (MPR) less than 1 (Figure S4 F), likely due to more skewed distributions of sgRNAs in the metastases compared to those in the late primary tumors. A small subset of sgRNAs, however, are more abundant in metastases than in primary tumors (MPR > 1) in multiple mice (e.g. sgRNAs targeting *Nf2*, *Trim72*, *Prostaglandin E Synthase 2 (Ptgse2)* or *Ubiquitin-conjugating enzyme E2G 2 (Ube2g2)*) (Figure 4F).

For four genes, *Nf2*, *Pten*, *Trim72*, and *Zfyve28*, two independent sgRNAs targeting different regions of the same gene were enriched in lung metastases (Figure 4G). One of the *Zfyve28*-targeting sgRNAs, however, is enriched in only one mouse; whereas *Nf2*, *Pten* and *Trim72* all have two sgRNAs enriched in multiple mice (Figure 4H). These three genes, several representative genes with one frequently enriched sgRNA (*Cdkn2a*, *Fga*, *Cryba4*), and the top two scoring microRNAs (*miR-152* and *miR-345*) were chosen to assay individually for primary tumor growth and metastases formation.

Validation *in vivo* using individual sgRNAs

For these eight genes (*Nf2*, *Pten*, *Trim72*, *Cdkn2a*, *Fga*, *Cryba4*, *miR-152* and *miR-345*), we cloned multiple sgRNAs targeting each of them into the lentiGuide-Puro vector, and transduced them into the Cas9-GFP KPD cell line (Figure 5A) (Experimental Procedures). As expected, these sgRNAs generated a broad distribution of NHEJ-mediated indels at the target site when examined three days post-transduction, with a bias toward deletions (Figure 5B). For protein coding genes, the majority (> 80%) of indels are out-of-frame, which potentially disrupt the protein functions. For *miR-152* and *miR-345*, the sgRNAs generated mostly deletions (> 90% of indels are deletions, average indel size = -7 bp) (Figure 5B), overlapping with the loop or mature microRNA sequences in the hairpins, which are structures required for maturation of microRNAs. For proteins where specific antibodies are available (*Nf2* and *Pten*), we found that the majority of the protein products were significantly reduced one week after lentiviral sgRNA infection (Figure S6 A).

When these single-sgRNA-transduced cells were transplanted into the flanks of immunocompromised mice, they all formed tumors *in situ*. With two mice injected per sgRNA and three sgRNAs per gene, all genes tested showed increased lung metastasis formation compared to controls (untransduced and non-targeting sgRNAs), with the most significant ones being *Nf2*, *Pten* and *Cdkn2a* (Fisher's exact test, one-tailed, $p < 10^{-3}$) (Figure 5C–D). *Fga* and *Trim72* also have effects on metastasis acceleration (*Fga*: $p = 0.001$, *Trim72*: $p = 0.046$). *Cryba4* is not statistically different from controls ($p = 0.1$). Both microRNAs targeted significantly increased metastasis (*miR-345*: $p = 0.01$, *miR-152*: $p = 0.046$). These data suggest that loss-of-function mutations in any of *Nf2*, *Pten*, *Cdkn2a*, *Trim72*, *Fga*, *miR345* or *miR-152* are sufficient to accelerate the rate of metastasis formation in this genetic background.

Most genes targeted by single sgRNAs also contributed to accelerated primary tumor growth compared to controls (Figure 5E). *Nf2* and *Pten* loss-of-function dramatically sped up tumor growth (KS test, $p < 0.001$) (Figure 5E); *Cdkn2a*-, *Trim72*- and *Fga*- targeting sgRNAs slightly accelerate primary tumor growth (KS test, $p = 0.003 - 0.01$); *Cryba4* has a marginal effect (KS test, $p = 0.08$); neither *miR-152*- nor *miR-345*- targeting sgRNAs promote

primary tumor growth (KS test, $p > 0.1$). Overall, for the targets we examined using individual sgRNAs, the number of lobes with lung metastases strongly correlates with the terminal volume of the late primary tumor (or average primary tumor growth rate) (correlation, $\rho = 0.83$, F-test, $p < 0.01$) (Figure 5F), indicating at a single gene level that mutant cells with a stronger ability to promote primary tumor growth generate metastases faster.

To analyze blood samples for the presence of circulating tumor cells (CTCs), we designed a microfluidic device based on the physical size of the Cas9-GFP KPD cells (Figure S6 B–C). We performed CTC capture with terminal blood samples from mice injected with Cas9-GFP KPD cells transduced with sgRNAs targeting *Nf2*, *Pten*, *Trim72*, *Cdkn2a*, *miR-152* and control cells (uninfected or non-targeting sgRNA) (Figure S6 C–D). Mice transplanted with cells transduced with sgRNAs targeting *Nf2*, *Pten*, *Trim72*, *Cdkn2a* or *miR-152* had a higher concentration of CTCs as compared to controls (Figure S6 D–G), consistent with the higher rate of lung metastasis formation.

Competitive dynamics of top hits assessed using an sgRNA minipool

To better understand the relative metastatic potential of multiple genes from our genome-wide screen, we designed a targeted pooled screen with a smaller library. This small library (termed validation minipool) contains 524 sgRNAs targeting 53 genes which had highly enriched sgRNAs in lung metastases in the genome-wide screen (10 sgRNAs per gene for most genes) plus 100 non-targeting sgRNAs. We also created a size-matched library containing 624 non-targeting sgRNAs (termed control minipool) (Figure 6A). Lentiviruses from these two pools were used to transduce the Cas9-GFP KPD cells, which were then cultured *in vitro* for one week, and then transplanted into *Nu/Nu* mice (Figure 6A). Both validation minipool and control minipool transduced cells induced primary tumor growth at a similar rate (Figure 6B). However, mice transplanted with validation minipool cells had a dramatically elevated rate of lung metastasis formation (Figure 6C).

We sequenced the validation minipool plasmid library, the transduced cells pre-transplantation, as well as the late stage primary tumors and whole lungs of the mice at 5 weeks post-transplantation. The sgRNA representations correlate strongly between technical replicates of the transduced cell pool, late primary tumor and lung metastases (Figure S7 A, D). The sgRNA representation in the cell sample strongly correlated with the plasmid (correlation, $\rho = 0.91$) (Figure S7 B, D). Almost all (99.4%) sgRNAs were recovered in the plasmid and the cell population (Figure S7 C). The late primary tumors retained less than half of the sgRNAs, while the metastases in the whole lung only retained a small fraction (2 – 7%) of all sgRNAs (Figure S7 C). Enriched sgRNAs from lung metastases clustered with each other and with late primary tumors (Figure S7 D). Similar to the genome-wide library, in this validation minipool, the plasmid and cell samples had a unimodal distribution of sgRNAs, whereas the late primary tumors and lung metastases contained a bi-modal distribution, with the majority of sgRNAs being absent and a small fraction spanning a large range of non-zero read counts (Figure 6D). Intriguingly, two mice retained relatively high sgRNA diversity in late primary tumors (Figure 6D), likely due to dormant or slowly proliferating cells that remained in low numbers during tumor growth. Similar to the

genome-wide library, large shifts in the sgRNA distribution exist between different sample types (KS test, $p < 10^{-15}$ for pairwise comparisons between the cell, primary tumor and lung metastases, $p = 0.02$ between plasmid and cell) (Figure 6E).

In the validation minipool, the sgRNAs detected in the late primary tumors or the lungs of five different mice significantly overlap with each other (Figure S7 E–F). The late primary tumors and lung metastases are dominated by a few sgRNAs (Figure 7A, Figure S7 G–I), suggesting these sgRNAs outcompete others during tumor growth and metastasis. In this small size validation library, the sgRNA representations are highly correlated between late primary tumors and lung metastases (correlation, $\rho = 0.55$ on average, F test, $p < 0.01$, $n = 5$) (Figure 7B). The late primary tumors and lung metastases have dozens of sgRNAs at moderate to high frequencies (Figure 7B–C). Several genes have multiple independent sgRNAs that are enriched in the lung over the primary tumor (MPR > 1), such as *Nf2* (8 sgRNAs), *Pten* (4 sgRNAs), *Trim72* (3 sgRNAs), *Ube2g2* (3 sgRNAs), *Ptges2* (2 sgRNAs) and *ATP-dependent DNA Ligase IV (Lig4)* (2 sgRNAs) (Figure 7C–D). Two *Cdkn2a* sgRNAs were present in both late primary tumors and lung metastases in two mice, but with MPR < 1. *Fga*-, *Cryba4*-, *miR-152*- or *miR-345*- targeting sgRNAs were not found at high frequency in either late primary tumors or lung metastases, which suggests that they are outcompeted by other loss-of-function mutations (such as *Nf2*), which agrees with the relatively reduced metastasis formation of these genes in the individual sgRNA validation. These results further validate several of the top hits from the primary screen, using either sgRNA dominance (e.g. *Nf2*, *Pten*, *Trim72*) or MPR (e.g. *Nf2*, *Trim72*, *Ube2g2*, *Ptges2*). This validation minipool reveals the dynamics of multiple competing mutants chosen from the primary screen hits, and indicates that mutants with strong pro-growth effects tend to enhance metastases (Figure 7E).

TCGA gene expression of screen hits in human lung cancer

To assess the relevance of our mGeCKOa and validation minipool screen hits (genes targeted by sgRNAs enriched in lung metastases) to pathological metastasis in human cancer, we performed gene expression analysis of the human orthologs of these genes. We compared mRNA levels in metastatic compared to non-metastatic primary tumors in patients samples using TCGA mRNA sequencing data. We found that most (61 – 75%) of these genes are downregulated in metastatic tumors in non-small cell lung cancer patients (Figure S5D–E, Table S6). These data suggest that downregulation of these genes is selected for in metastatic tumors from patients.

Discussion

Pooled mutagenesis in a metastasis model

Distal metastases develop as primary tumors shed circulating tumor cells (CTCs) into the circulation, from which CTCs travel to the destination site, move out of the blood vessels and initiate clonal growth (Valastyan and Weinberg, 2011; Vanharanta and Massague, 2013; Weinberg, 2007). In this study, cancer cells transplanted into the flanks of mice form primary tumors *in situ*, and cells from this mass undergo the intravasation – circulation - extravasation - clonal growth cascade to form distal metastases (Francia et al., 2011). The

initial lung cancer cell line has little capacity to form metastases; in contrast, after being mutagenized with the mGeCKOa genome-scale Cas9 knockout library, the cell population form highly metastatic tumors. Thus, these mutations, acting in simple or complex, pleiotropic ways, accelerate metastasis. In this model, the effect of mutations on metastasis strongly correlates with their abundance in late stage primary tumors.

SgRNA dynamics during tumor evolution

The dynamics of the sgRNA population changed dramatically over the course of tumor development and metastasis, reflecting the selection and bottlenecks of cellular evolution *in vitro* and *in vivo*. After a week in culture, cells retained most of the sgRNAs present in the plasmid library, with decreases in sgRNAs targeting genes involved in fundamental cellular processes. The distribution of non-targeting control sgRNAs is almost identical to those targeting genes, suggesting that the selective pressure of *in vitro* culture alone does not radically alter sgRNA representation, which is similar to previous observations in human melanoma cells (Shalem et al., 2014).

In contrast, less than half of the sgRNAs survive in an early stage primary tumor. This loss of representation occurs with both gene-targeting sgRNAs and non-targeting control sgRNAs, suggesting that random-sampling influences the sgRNA dynamics during the transplantation and tumor initiation processes, although we cannot exclude that some of the non-targeting sgRNAs might have detrimental or pro-growth effects. We also detected further dropout of genes involved in fundamental cellular processes in early tumor samples compared to cell samples. Thus, it is likely that the sgRNA dynamics are influenced by a combination of selection and random sampling during transplantation and tumor initiation.

As primary tumors grow, the mutant cells proliferate and compete as a pool. This creates strong selection for sgRNAs targeting anti-apoptotic genes and other tumor suppressors. The majority of the genetic diversity in early tumors is lost during the subsequent 4 weeks of primary tumor growth. Accordingly, sequencing revealed a smaller set of dominant sgRNAs, usually on the order of hundreds to a few thousand per mouse. In addition, almost all of non-targeting sgRNAs are lost during primary tumor growth, which is consistent with selection for cells with special growth and survival properties. This observation is also consistent with earlier transplantation studies by Kerbel and colleagues using small pools of randomly mutagenized cells, which found that the majority of clonal variants detectable by Southern blot disappeared within six weeks of primary tumor growth, leaving one dominant clone (Korzak et al., 1988; Waghorne et al., 1988).

Each step towards metastasis acts as a bottleneck. In the lung metastases, we detected very few sgRNAs at high abundance. As with the primary tumor, we find only a few non-targeting sgRNAs at low frequencies in metastases. Their presence could be due to unknown off-target effects of these sgRNAs, or random shedding of CTCs in the primary tumor, or clustering together with other strongly selected CTCs during metastasis (Aceto et al., 2014).

Relevance of screen hits to human cancer

Several of the genes enriched in late stage primary tumors are associated with cancer, but their functions in tumor growth are poorly understood. For example, *Mgmt*, a gene with two enriched sgRNAs, is required for DNA repair and thus crucial for genome stability (Tano et al., 1990). Mutation, silencing or promoter methylation of *MGMT* is associated with primary glioblastomas (Jesien-Lewandowicz et al., 2009). *Med16*, another gene with two enriched sgRNAs, encodes a subunit of the mediator complex of transcription regulation, which has been recently implicated in cancer (Huang et al., 2012; Schiano et al., 2014).

We found that the genes that are significantly enriched in lung metastases largely overlap with those found in abundance in the late primary tumor. Several of these hits were validated *in vivo* using multiple individual sgRNAs, including *Nf2*, *Pten*, *Cdkn2a*, *Trim72*, *Fga*, *miR-152* and *miR-345*. *Nf2*, *Pten* and *Cdkn2a* are well-known tumor suppressor genes. Intriguingly, the *NF2* locus is only mutated at a 1% frequency in primary tumors of human NSCLC patients (LUAD and/or LUSC) (TCGA-Network, 2012, 2014). It is possible that *NF2* mutations influence metastases to a greater degree than primary tumor growth, but this awaits metastasis genomics from patient samples. *Pten* mutations are also associated with advanced stages of tumor progression in a mouse model of lung cancer (McFadden et al., 2014), and *PTEN* was found mutated at 8% in adenocarcinoma patients (LUAD). *CDKN2A* has been shown to be often inactivated in lung cancer (Kaczmarczyk et al., 2012; Yokota et al., 2003). For *Trim72* (an E3 ubiquitin ligase) and *Fga* (the extracellular matrix protein fibrinogen involved in blood clot formation), there is little information associating them to metastasis or cancer. Studies have shown that *miR-152* and *miR-345* are associated with cancer and metastasis (Cheng et al., 2014; Tang et al., 2011). *FGF2* and *BAG3*, which promote metastasis, were predicted targets of *miR-152* and *miR-345*, thus loss of these microRNAs may lead to acceleration of metastases likely due to de-repression of these genes (Cheng et al., 2014; Tang et al., 2011).

In our own analysis of TCGA samples from lung cancer patients, we observed downregulation of the human orthologs of the genes identified in the genome-wide and validation minipool screens at the mRNA level in metastatic tumors compared to non-metastatic tumors (Figure S5D–E, Table S6, Supplemental Results and Discussion), suggesting that these genes may also be inactivated during pathological metastasis. Human orthologs of these genes are often found mutated in cancers (Figure S5A–C). Moreover, these genes have been implicated in various pathways and biological processes in tumorigenesis and/or metastasis in human cancer (Table S7A–C). However, most cancer sequencing studies involve samples from primary tumors of patients. In the clinic, metastases are rarely sampled. Future patient sequencing directly from metastases may further connect genes identified in the mouse model to those mutated or silenced in clinical metastases.

Future *in vivo* functional genomic screens

Our study provides a roadmap for *in vivo* Cas9 screens and future studies can take advantage of this model to explore other oncogenotypes, delivery methods or metastasis target organs. Genome-scale CRISPR screening is feasible using a transplant model with virtually any cell

line or genetic background (e.g. mutations in *EGFR*, *KRAS*, *ALK*, etc.), including a large repertoire of human cell lines from diverse cancer types (Barretina et al., 2012). Other cell delivery methods, such as intravenous injection or orthotopic transplantation, may help identify genes regulating extravasation and clonalization. Examining samples from other stages or sites, such as CTCs or metastases to other organs can provide a more refined picture of tumor evolution.

In addition to these parameters, several aspects of the screen perturbations themselves can also be modified. Targeted drug therapies or immunotherapies can be applied in conjunction with the *in vivo* screening strategy to identify genes involved in acquired resistance. Recent advances in screen technology, such as Cas9-mediated activation (Gilbert et al., 2014; Konermann et al., 2014), may be used to identify metastasis-regulating factors that act in a gain-of-function manner. Activation screens that identify oncogenes, as well as dropout screens that identify genetic dependencies, may facilitate identification of novel therapeutic targets. Targeted subpool strategies can be used to reduce the library size and facilitate further confirmation of primary screens. In a customized library, genes can be chosen based on genomic analysis, pathways, or clinical relevance for focused screening libraries. Additionally, application of pooled sgRNA libraries using individually barcoded cells will allow quantitative assessment of the robustness and significance of each candidate hit as well as enable analysis of the competitive dynamics amongst different perturbations. Taken together, Cas9-based *in vivo* screening establishes a new platform for functional genomic discovery.

Experimental Procedures

Generation of Cas9-GFP expression vector

A lentiviral vector, lenti-Cas9-NLS-FLAG-2A-EGFP (lentiCas9-EGFP), was generated by subcloning Cas9 into a lentiviral vector.

Pooled guide-only library cloning and viral production

The Cas9-GFP KPD cell line was transduced at a MOI of ~ 0.4 with a genome-wide lentiviral mouse CRISPR knockout guide-only library (Sanjana et al., 2014) containing 67,405 sgRNAs (mGeCKOa, Addgene 100000053) with at least 400-fold representation (cells per construct) in each infection replicate.

Animal work statement

All animal work was performed under the guidelines of Division of Comparative Medicine (DCM), with protocols (0411-040-14, 0414-024-17, 0911-098-11, 0911-098-14 and 0914-091-17) approved by Massachusetts Institute of Technology Committee for Animal Care (CAC), and were consistent with the Guide for Care and Use of Laboratory Animals, National Research Council, 1996 (institutional animal welfare assurance no. A-3125-01).

Mice, tumor transplant and metastasis analysis in the primary screen

Untransduced or mGeCKOa-transduced Cas9-GFP KPD cells were injected subcutaneously into the right side flank of *Nu/Nu* mice at 3×10^7 cells per mouse. Transplanted primary

tumor sizes were measured by caliper. At 6 weeks post transplantation, mice were sacrificed and several organs (liver, lung, kidney and spleen) were dissected for examination of metastases under a fluorescent stereoscope.

Mouse tissue collection

Primary tumors and other organs were dissected manually. For molecular biology, tissues were flash frozen with liquid nitrogen, ground in 24 Well Polyethylene Vials with metal beads in a GenoGrinder machine (OPS diagnostics). Homogenized tissues were used for DNA/RNA/protein extractions using standard molecular biology protocols. Tissues for histology were then fixed in 4% formaldehyde or 10% formalin overnight, embedded in paraffin, and sectioned at 6 μm with a microtome as described previously (Chen et al., 2014). Slices were subjected to hematoxylin and eosin (H&E) staining as described previously (Chen et al., 2014).

Genomic DNA extraction from cells and mouse tissues

Genomic DNA from cells and tissues (primary tumors and lungs) were extracted using a homemade modified salt precipitation method similar to the Puregene (Qiagen/Gentra) procedure. The sgRNA cassette was amplified and prepared for Illumina sequencing as previously described (Shalem et al., 2014). A detailed readout protocol can be found in Extended Experimental Procedures.

Individual gene and microRNA validation

Six sgRNAs per protein coding gene and four sgRNAs per microRNA gene were chosen for validation using individual sgRNAs (Table S4). For protein coding genes, we cloned gene. For microRNAs, we used all 4 sgRNAs from the mGeCKOa library.

Validation and control minipool synthesis and in vivo transplantation

Validation and control minipools (Tables S5) were synthesized using array oligonucleotide synthesis (CustomArray) and transduced at >1000-fold representation in Cas9-GFP KPD cells. After 7 days in culture, Cas9-GFP KPD cells transduced with the validation minipool or control minipool were injected subcutaneously into the right side flank of *Nu/Nu* mice at 3×10^7 cells per mouse with 5 replicate mice. After five weeks, mice were sacrificed, and primary tumors and lungs were dissected.

Supplementary Material

Refer to Web version on PubMed Central for supplementary material.

Acknowledgments

We thank R. Weinberg for critically reading the manuscript; the entire Sharp laboratory and Zhang laboratory, L. Cong, T. Kelly, X. Ni, M. Nobel, J. Boehm, A. Tsherniak, S. Levine, M. Cornwall-Brady, S. Malstrom, M. Jennings, E. Vasile, C. Whittaker, K. Cormier, R. Bronson and colleagues in the Koch Institute, Broad Institute, McGovern Institute and Department of Biology for technical assistance and/or discussion; the Swanson Biotechnology Center for technical support (Genomics, Animal Imaging & Preclinical Testing, Bioinformatics and Computing, Microscopy, Flow Cytometry, Microscopy and Histology, in particular). This work is supported by grants to P.A.S., including a United States Public Health Service grant R01-CA133404 from the National Institutes of Health, an MIT-Harvard Center for Cancer Nanotechnology Excellence Grant U54 CA151884 from the National

Cancer Institute, a generous gift from the Marie D. and Pierre Casimir-Lambert Fund, an SkTech/MIT Initiative Grant from the Skolkovo Foundation, and the Koch Institute Support (core) grant P30-CA14051 from the National Cancer Institute. F.Z. is supported by the National Institutes of Health through (NIMH: 5DP1-MH100706) and (NIDDK: 5R01-DK097768), a Waterman Award from the National Science Foundation, the Keck, New York Stem Cell, Damon Runyon, Searle Scholars, Merkin, and Vallee Foundations, and Bob Metcalfe. F.Z. is a New York Stem Cell Foundation Robertson Investigator. S.C. is a Damon Runyon Cancer Research Fellow (DRG-2117-12) and also supported by the Dale Frey Award for Breakthrough Scientists. N.E.S. is supported by a Simons Center for the Social Brain Postdoctoral Fellowship and NIH NHGRI award K99-HG008171. O.S. is a fellow of the Klarman Cell Observatory. R.W. is supported by an NIH grant U54 CA151884. D.A.S. is supported by a NSF Graduate Research Fellowship. H.L. is supported by DOD grant OCRP W81XWH-14-1-0279. CRISPR reagents (plasmids, libraries) are available to the academic community through Addgene.

References

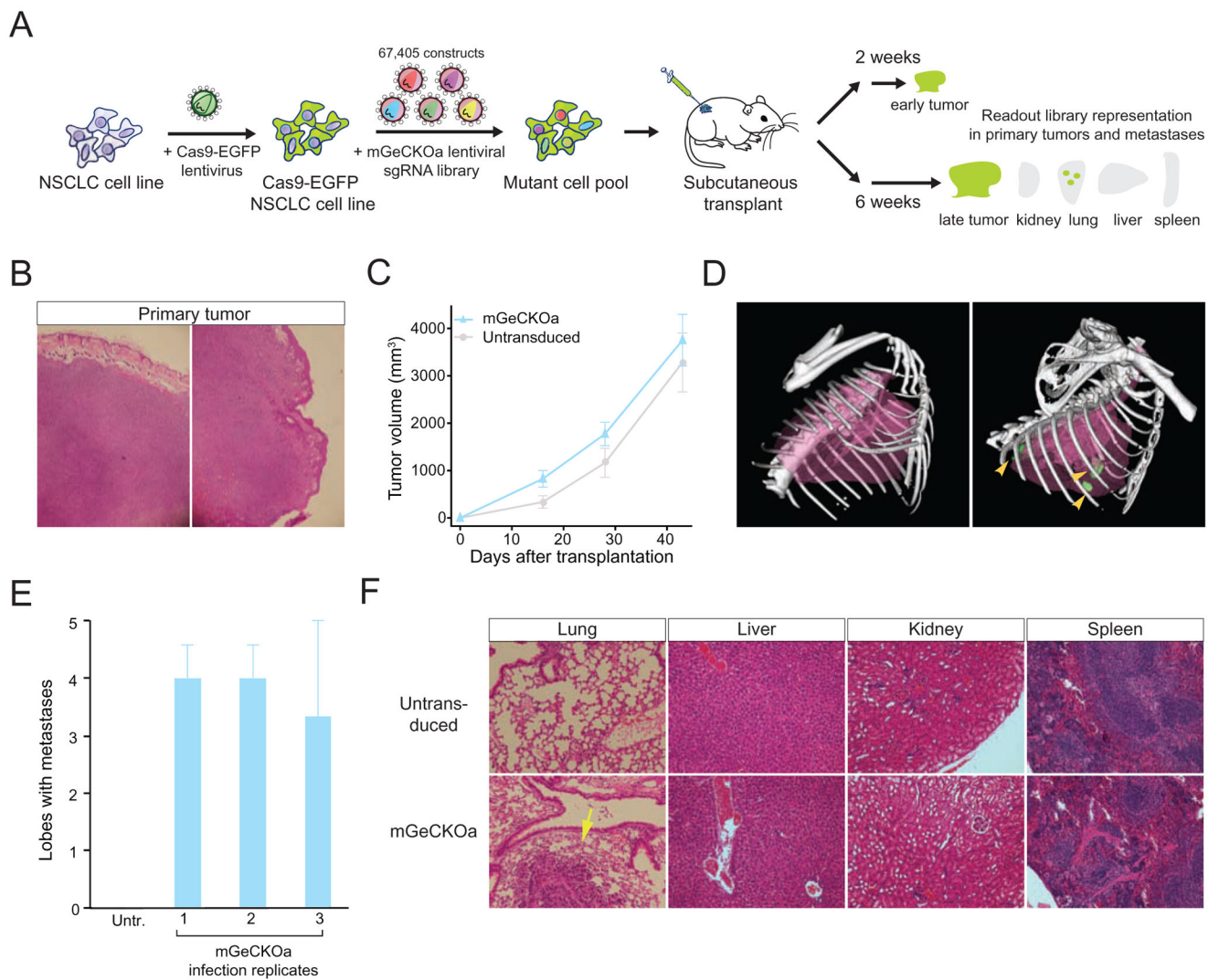
- Aceto N, Bardia A, Miyamoto DT, Donaldson MC, Wittner BS, Spencer JA, Yu M, Pely A, Engstrom A, Zhu H, et al. Circulating tumor cell clusters are oligoclonal precursors of breast cancer metastasis. *Cell*. 2014; 158:1110–1122. [PubMed: 25171411]
- Barrangou R, Fremaux C, Deveau H, Richards M, Boyaval P, Moineau S, Romero DA, Horvath P. CRISPR provides acquired resistance against viruses in prokaryotes. *Science*. 2007; 315:1709–1712. [PubMed: 17379808]
- Barretina J, Caponigro G, Stransky N, Venkatesan K, Margolin AA, Kim S, Wilson CJ, Lehar J, Kryukov GV, Sonkin D, et al. The Cancer Cell Line Encyclopedia enables predictive modelling of anticancer drug sensitivity. *Nature*. 2012; 483:603–607. [PubMed: 22460905]
- Bolotin A, Quinquis B, Sorokin A, Ehrlich SD. Clustered regularly interspaced short palindrome repeats (CRISPRs) have spacers of extrachromosomal origin. *Microbiology*. 2005; 151:2551–2561. [PubMed: 16079334]
- Cerami E, Gao J, Dogrusoz U, Gross BE, Sumer SO, Aksoy BA, Jacobsen A, Byrne CJ, Heuer ML, Larsson E, et al. The cBio cancer genomics portal: an open platform for exploring multidimensional cancer genomics data. *Cancer discovery*. 2012; 2:401–404. [PubMed: 22588877]
- Chen S, Xue Y, Wu X, Le C, Bhutkar A, Bell EL, Zhang F, Langer R, Sharp PA. Global microRNA depletion suppresses tumor angiogenesis. *Genes & development*. 2014; 28:1054–1067. [PubMed: 24788094]
- Cheng Z, Ma R, Tan W, Zhang L. MiR-152 suppresses the proliferation and invasion of NSCLC cells by inhibiting FGF2. *Experimental & molecular medicine*. 2014; 46:e112. [PubMed: 25190353]
- Chylinski K, Le Rhun A, Charpentier E. The tracrRNA and Cas9 families of type II CRISPR-Cas immunity systems. *RNA biology*. 2013; 10:726–737. [PubMed: 23563642]
- Chylinski K, Makarova KS, Charpentier E, Koonin EV. Classification and evolution of type II CRISPR-Cas systems. *Nucleic acids research*. 2014; 42:6091–6105. [PubMed: 24728998]
- Cong L, Ran FA, Cox D, Lin S, Barretto R, Habib N, Hsu PD, Wu X, Jiang W, Marraffini LA, et al. Multiplex genome engineering using CRISPR/Cas systems. *Science*. 2013; 339:819–823. [PubMed: 23287718]
- Deltcheva E, Chylinski K, Sharma CM, Gonzales K, Chao Y, Pirzada ZA, Eckert MR, Vogel J, Charpentier E. CRISPR RNA maturation by trans-encoded small RNA and host factor RNase III. *Nature*. 2011; 471:602–607. [PubMed: 21455174]
- Francia G, Cruz-Munoz W, Man S, Xu P, Kerbel RS. Mouse models of advanced spontaneous metastasis for experimental therapeutics. *Nature reviews Cancer*. 2011; 11:135–141.
- Gao J, Aksoy BA, Dogrusoz U, Dresdner G, Gross B, Sumer SO, Sun Y, Jacobsen A, Sinha R, Larsson E, et al. Integrative analysis of complex cancer genomics and clinical profiles using the cBioPortal. *Science signaling*. 2013; 6:p11. [PubMed: 23550210]
- Garneau JE, Dupuis ME, Villion M, Romero DA, Barrangou R, Boyaval P, Fremaux C, Horvath P, Magadan AH, Moineau S. The CRISPR/Cas bacterial immune system cleaves bacteriophage and plasmid DNA. *Nature*. 2010; 468:67–71. [PubMed: 21048762]
- Garraway LA, Lander ES. Lessons from the cancer genome. *Cell*. 2013; 153:17–37. [PubMed: 23540688]

- Gasiunas G, Barrangou R, Horvath P, Siksnys V. Cas9-crRNA ribonucleoprotein complex mediates specific DNA cleavage for adaptive immunity in bacteria. *Proceedings of the National Academy of Sciences of the United States of America*. 2012; 109:E2579–2586. [PubMed: 22949671]
- Gilbert LA, Horlbeck MA, Adamson B, Villalta JE, Chen Y, Whitehead EH, Guimaraes C, Panning B, Ploegh HL, Bassik MC, et al. Genome-Scale CRISPR-Mediated Control of Gene Repression and Activation. *Cell*. 2014; 159:647–661. [PubMed: 25307932]
- Hanahan D, Weinberg RA. Hallmarks of cancer: the next generation. *Cell*. 2011; 144:646–674. [PubMed: 21376230]
- Heimann R, Hellman S. Aging, progression, and phenotype in breast cancer. *Journal of clinical oncology : official journal of the American Society of Clinical Oncology*. 1998; 16:2686–2692. [PubMed: 9704718]
- Hsu PD, Scott DA, Weinstein JA, Ran FA, Konermann S, Agarwala V, Li Y, Fine EJ, Wu X, Shalem O, et al. DNA targeting specificity of RNA-guided Cas9 nucleases. *Nature biotechnology*. 2013; 31:827–832.
- Huang S, Holzel M, Knijnenburg T, Schlicker A, Roepman P, McDermott U, Garnett M, Grenrum W, Sun C, Prahallad A, et al. MED12 controls the response to multiple cancer drugs through regulation of TGF-beta receptor signaling. *Cell*. 2012; 151:937–950. [PubMed: 23178117]
- Jesien-Lewandowicz E, Jesionek-Kupnicka D, Zawlik I, Szybka M, Kulczycka-Wojdala D, Rieske P, Sieruta M, Jaskolski D, Och W, Skowronski W, et al. High incidence of MGMT promoter methylation in primary glioblastomas without correlation with TP53 gene mutations. *Cancer genetics and cytogenetics*. 2009; 188:77–82. [PubMed: 19100509]
- Jinek M, Chylinski K, Fonfara I, Hauer M, Doudna JA, Charpentier E. A programmable dual-RNA-guided DNA endonuclease in adaptive bacterial immunity. *Science*. 2012; 337:816–821. [PubMed: 22745249]
- Kaczmarczyk G, Lewandowski R, Trautsolt W, Ziolkowski A, Kozielski J. Cytological examination of pleural cavity lavage accompanied by the study of gene promoter hypermethylation of p16 and O6-methylguanine-DNA-methyltransferase genes in diagnostics of non-small cell lung cancer metastatic changes into pleura. *Contemporary oncology*. 2012; 16:322–327. [PubMed: 23788902]
- Koike-Yusa H, Li Y, Tan EP, del Velasco-Herrera MC, Yusa K. Genome-wide recessive genetic screening in mammalian cells with a lentiviral CRISPR-guide RNA library. *Nature biotechnology*. 2014; 32:267–273.
- Konermann S, Brigham MD, Trevino AE, Joung J, Abudayyeh OO, Barcena C, Hsu PD, Habib N, Gootenberg JS, Nishimasu H, et al. Genome-scale transcriptional activation by an engineered CRISPR-Cas9 complex. *Nature*. 2014
- Korczak B, Robson IB, Lamarche C, Bernstein A, Kerbel RS. Genetic tagging of tumor cells with retrovirus vectors: clonal analysis of tumor growth and metastasis in vivo. *Molecular and cellular biology*. 1988; 8:3143–3149. [PubMed: 3211140]
- Kumar MS, Pester RE, Chen CY, Lane K, Chin C, Lu J, Kirsch DG, Golub TR, Jacks T. Dicer1 functions as a haploinsufficient tumor suppressor. *Genes & development*. 2009; 23:2700–2704. [PubMed: 19903759]
- Lawrence MS, Stojanov P, Polak P, Kryukov GV, Cibulskis K, Sivachenko A, Carter SL, Stewart C, Mermel CH, Roberts SA, et al. Mutational heterogeneity in cancer and the search for new cancer-associated genes. *Nature*. 2013; 499:214–218. [PubMed: 23770567]
- Mali P, Yang LH, Esvelt KM, Aach J, Guell M, DiCarlo JE, Norville JE, Church GM. RNA-Guided Human Genome Engineering via Cas9. *Science*. 2013; 339:823–826. [PubMed: 23287722]
- McFadden DG, Papagiannakopoulos T, Taylor-Weiner A, Stewart C, Carter SL, Cibulskis K, Bhutkar A, McKenna A, Dooley A, Vernon A, et al. Genetic and clonal dissection of murine small cell lung carcinoma progression by genome sequencing. *Cell*. 2014; 156:1298–1311. [PubMed: 24630729]
- Nguyen DX, Bos PD, Massague J. Metastasis: from dissemination to organ-specific colonization. *Nature reviews Cancer*. 2009; 9:274–284.
- Rouet P, Smih F, Jasim M. Introduction of double-strand breaks into the genome of mouse cells by expression of a rare-cutting endonuclease. *Molecular and cellular biology*. 1994; 14:8096–8106. [PubMed: 7969147]

- Sanjana NE, Shalem O, Zhang F. Improved vectors and genome-wide libraries for CRISPR screening. *Nature Methods*. 2014; 11:783–784. [PubMed: 25075903]
- Sapranaukas R, Gasiunas G, Fremaux C, Barrangou R, Horvath P, Siksnyš V. The *Streptococcus thermophilus* CRISPR/Cas system provides immunity in *Escherichia coli*. *Nucleic acids research*. 2011; 39:9275–9282. [PubMed: 21813460]
- Schiano C, Casamassimi A, Rienzo M, de Nigris F, Sommese L, Napoli C. Involvement of Mediator complex in malignancy. *Biochimica et biophysica acta*. 2014; 1845:66–83. [PubMed: 24342527]
- Schramek D, Sendoel A, Segal JP, Beronja S, Heller E, Oristian D, Reva B, Fuchs E. Direct in vivo RNAi screen unveils myosin IIa as a tumor suppressor of squamous cell carcinomas. *Science*. 2014; 343:309–313. [PubMed: 24436421]
- Shalem O, Sanjana NE, Hartenian E, Shi X, Scott DA, Mikkelsen TS, Heckl D, Ebert BL, Root DE, Doench JG, et al. Genome-scale CRISPR-Cas9 knockout screening in human cells. *Science*. 2014; 343:84–87. [PubMed: 24336571]
- Shao DD, Xue W, Krall EB, Bhutkar A, Piccioni F, Wang X, Schinzel AC, Sood S, Rosenbluh J, Kim JW, et al. KRAS and YAP1 converge to regulate EMT and tumor survival. *Cell*. 2014; 158:171–184. [PubMed: 24954536]
- Tang JT, Wang JL, Du W, Hong J, Zhao SL, Wang YC, Xiong H, Chen HM, Fang JY. MicroRNA 345, a methylation-sensitive microRNA is involved in cell proliferation and invasion in human colorectal cancer. *Carcinogenesis*. 2011; 32:1207–1215. [PubMed: 21665895]
- Tano K, Shiota S, Collier J, Foote RS, Mitra S. Isolation and structural characterization of a cDNA clone encoding the human DNA repair protein for O6-alkylguanine. *Proceedings of the National Academy of Sciences of the United States of America*. 1990; 87:686–690. [PubMed: 2405387]
- TCGA-Network. Comprehensive genomic characterization of squamous cell lung cancers. *Nature*. 2012; 489(7417):519–25. [PubMed: 22960745]
- TCGA-Network. Comprehensive molecular profiling of lung adenocarcinoma. *Nature*. 2014 Published online 09 July 2014.
- Valastyan S, Weinberg RA. Tumor metastasis: molecular insights and evolving paradigms. *Cell*. 2011; 147:275–292. [PubMed: 22000009]
- Vanharanta S, Massague J. Origins of metastatic traits. *Cancer cell*. 2013; 24:410–421. [PubMed: 24135279]
- Waghorne C, Thomas M, Lagarde A, Kerbel RS, Breitman ML. Genetic evidence for progressive selection and overgrowth of primary tumors by metastatic cell subpopulations. *Cancer research*. 1988; 48:6109–6114. [PubMed: 3167857]
- Wang T, Wei JJ, Sabatini DM, Lander ES. Genetic Screens in Human Cells Using the CRISPR-Cas9 System. *Science*. 2014; 343:80–84. [PubMed: 24336569]
- Weinberg, RA. *The biology of cancer*. New York: Garland Science; 2007.
- Yokota J, Nishioka M, Tani M, Kohno T. Genetic alterations responsible for metastatic phenotypes of lung cancer cells. *Clinical & experimental metastasis*. 2003; 20:189–193. [PubMed: 12741677]
- Zender L, Xue W, Zuber J, Semighini CP, Krasnitz A, Ma B, Zender P, Kubicka S, Luk JM, Schirmacher P, et al. An oncogenomics-based in vivo RNAi screen identifies tumor suppressors in liver cancer. *Cell*. 2008; 135:852–864. [PubMed: 19012953]
- Zhou Y, Zhu S, Cai C, Yuan P, Li C, Huang Y, Wei W. High-throughput screening of a CRISPR/Cas9 library for functional genomics in human cells. *Nature*. 2014; 509:487–491. [PubMed: 24717434]

Highlights

- Genome-wide *in vivo* screen using CRISPR/Cas9 in a mouse model of lung metastasis
- Identified loss-of-function mutations in known tumor suppressors and novel genes
- Targeted subpool as a pooled competition assay to validate genes from screen
- The effect of mutations on metastasis correlates with primary tumor abundance

**Figure 1.**

(A) Schematic representation of the loss-of-function metastasis screen using the mouse genome-scale CRISPR/Cas9 knock-out library (mGeCKOa).

(B) Representative hematoxylin and eosin (H&E) stains of primary tumor from *Nu/Nu* mice subcutaneously transplanted with a Cas9-GFP *Kras*^{G12D/+}; *p53*^{-/-}; *Dicer1*^{+/-} (KPD) NSCLC cell line, untransduced or transduced mGeCKOa lentiviral library. Scale bar: 200 μ m.

(C) Primary tumor growth curve of *Nu/Nu* mice transplanted with untransduced cells ($n = 3$ mice) or mGeCKOa-transduced Cas9-GFP KPD cells ($n = 9$ mice).

(D) Micro-CT 3D reconstruction of the lungs of representative mice transplanted with control (untransduced) and mGeCKOa-transduced (mGeCKOa) cell pools. Lung metastases were identified and traced in each 2D section (green).

(E) Percent of lobes with metastases visible after dissection under a fluorescence stereoscope, in *Nu/Nu* mice transplanted with untransduced Cas9-GFP KPD cells ($n = 3$ mice).

mice), or mGeCKOa-transduced Cas9-GFP KPD cells with three independent infection replicate experiments (R1, R2 and R3, $n = 3$ mice per replicate).

(F) Representative H&E stains from various organs of *Nu/Nu* mice subcutaneously transplanted with untransduced and mGeCKOa-transduced Cas9-GFP KPD cells. Yellow arrow indicates a lung metastasis. Scale bar: 40 μm .

(See also: Figure S1)

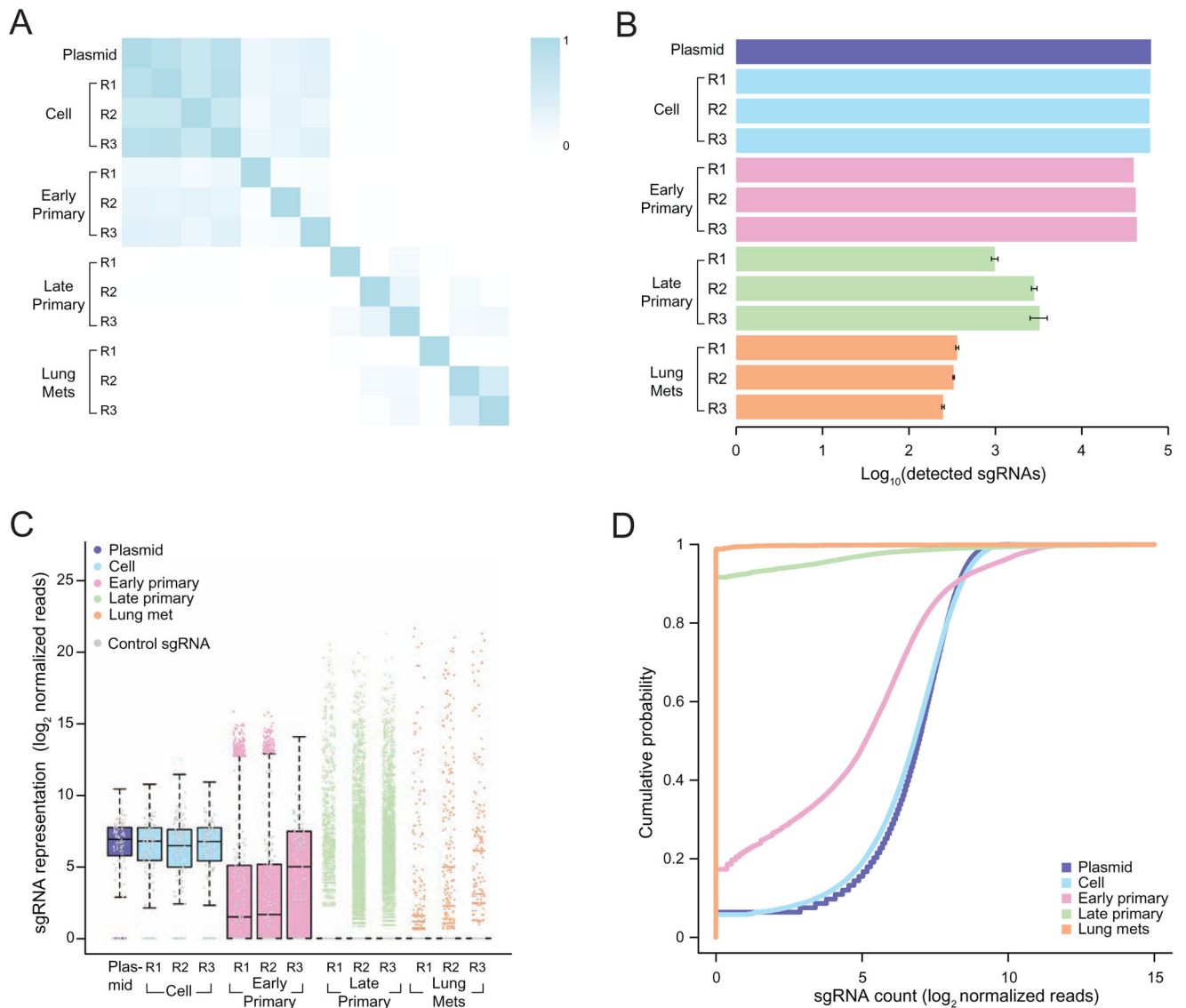


Figure 2.

(A) Pearson correlation coefficient of the normalized sgRNA read counts from the mGeCKOa plasmid library, transduced cells before transplantation (day 7 after spinfection), early primary tumors (~ 2 weeks after transplantation), late primary tumors (~ 6 weeks after transplantation), and lung metastases (~ 6 weeks after transplantation). For each biological sample type, 3 independent infection replicates (R1, R2 and R3) are shown. $n = 1$ mouse per infection replicate for early primary tumors and $n = 3$ mice per infection replicate for late primary tumors and lung samples.

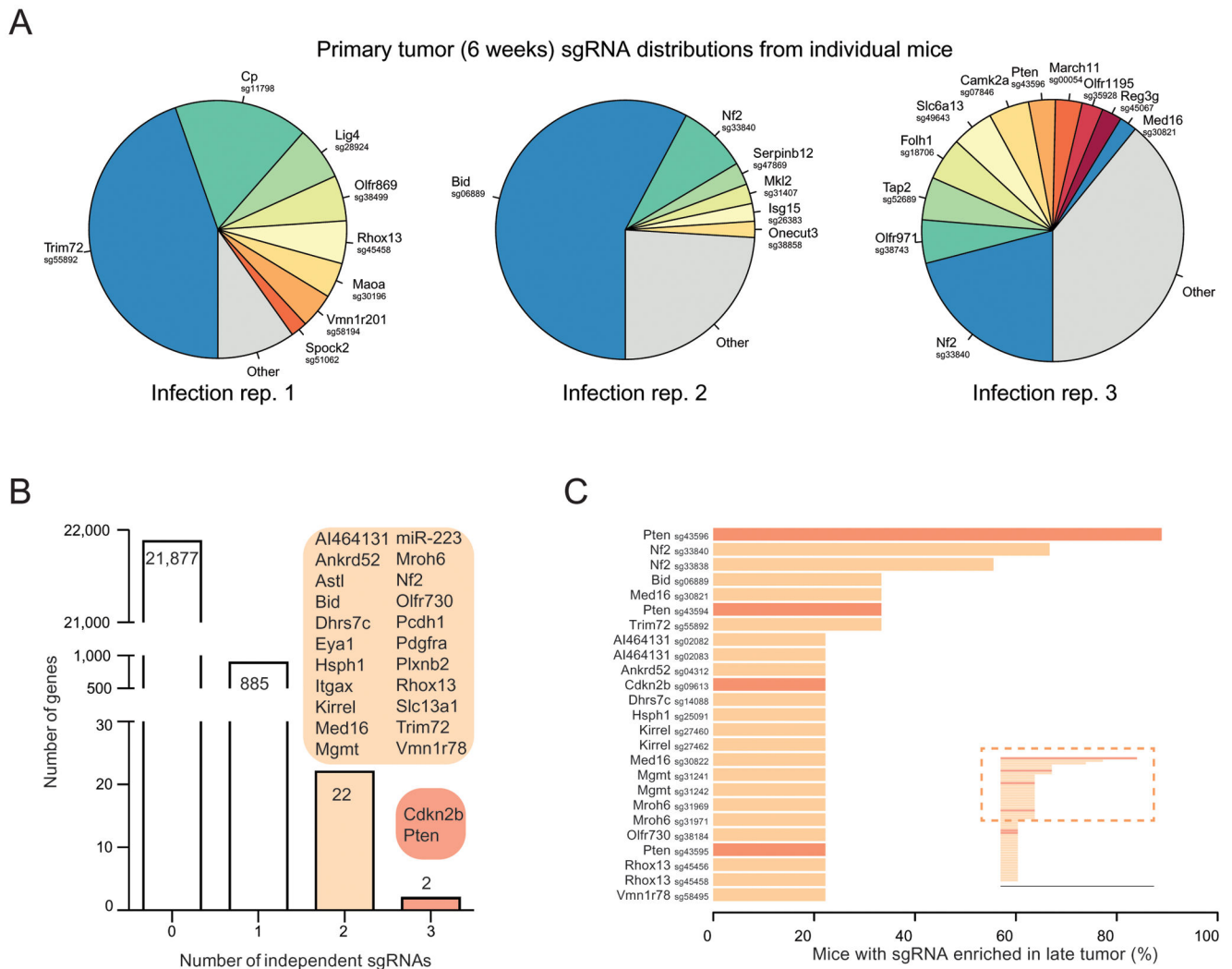
(B) Number of unique sgRNAs in the plasmid, cells before transplantation, early and late primary tumors and lung metastases as in (A), Error bars for late primary tumors and lung metastases denote the s.e.m. for $n = 3$ mice per infection replicate.

(C) Boxplot of the sgRNA normalized read counts for the mGeCKOa plasmid pool, cells before transplantation, early and late primary tumors and lung metastases as in (A). Outliers

are shown as colored dots for each respective sample. Gray dots overlaid on each boxplot indicate read counts for the 1,000 control (non-targeting) sgRNAs in the mGeCKOa library. Distributions for late primary tumors and lung metastases are averaged across individual mice from the same infection replication.

(D) Cumulative probability distribution of library sgRNAs in the plasmid, cells before transplantation, early and late primary tumors and lung metastases as in (A). Distributions for each sample type are averaged across individual mice and infection replications.

(See also: Figures S2 and S3)

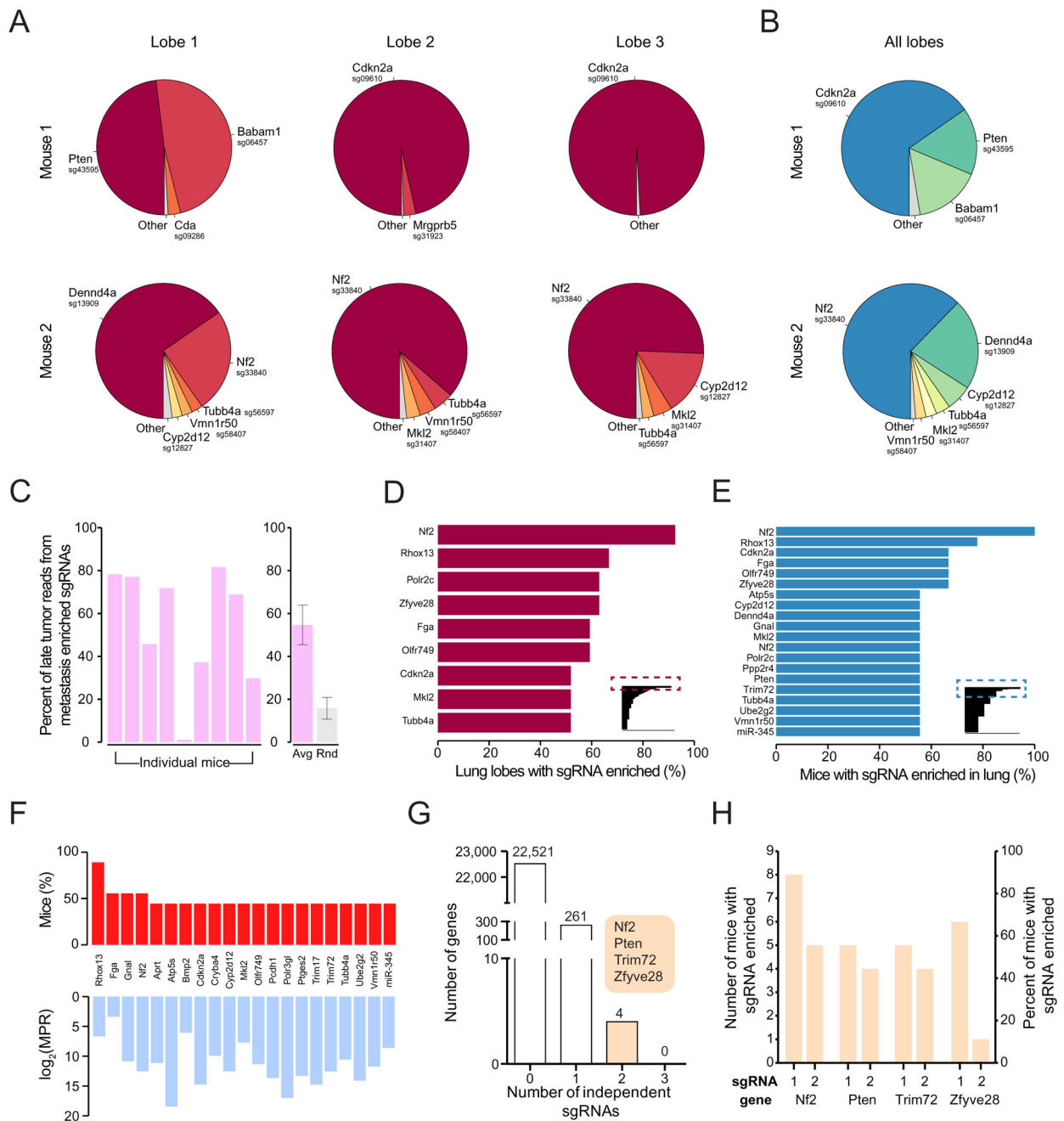
**Figure 3.**

(A) Pie charts of the most abundant sgRNAs in the primary tumors (at ~6 weeks post-transplantation) of three representative mice (one from each replicate mGeCKOa infection). The area for each sgRNA corresponds to the fraction of total reads from the primary tumor for the sgRNA. All sgRNAs with $\geq 2\%$ of total reads are plotted individually.

(B) Number of genes with 0, 1, 2 or 3 significantly enriched (FDR $< 0.2\%$ for at least one mouse) mGeCKOa sgRNAs targeting that gene. For genes/miRs with 2 or more enriched sgRNAs, genes/miRs are categorized by how many sgRNAs targeting that gene/miRs are enriched as indicated in the colored bubbles adjacent to each bar.

(C) *Inset*: Waterfall plot of sgRNAs where multiple sgRNAs targeting the same gene are significantly enriched in primary tumors. Each sgRNA is ranked by the percent of mice in which it is enriched. Only sgRNAs enriched in 2 or more mice are shown in the main panel. *Main panel*: Enlargement and gene labels for sgRNAs at the top of the list from the inset (boxed region).

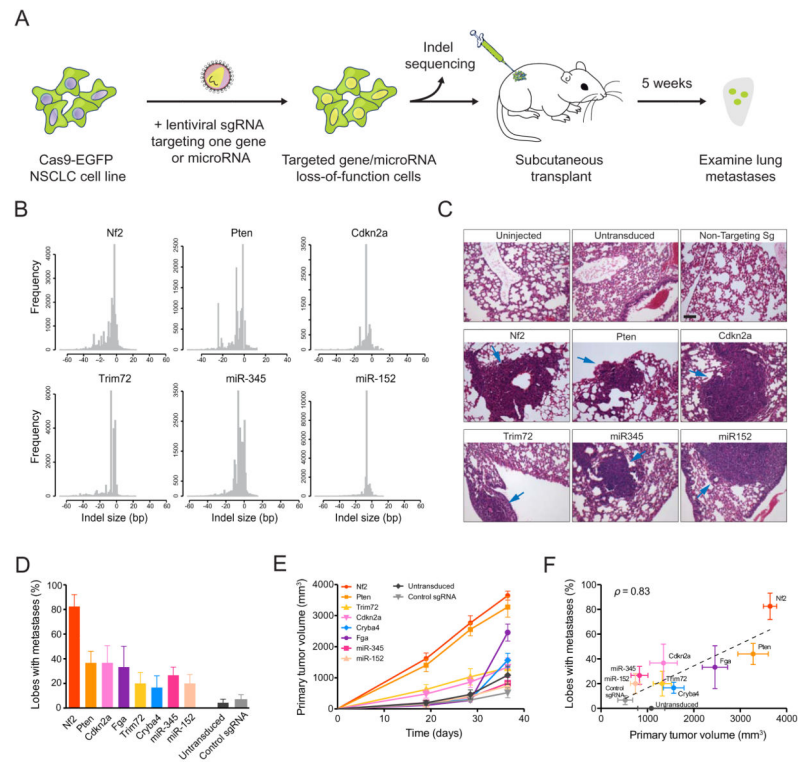
(See also: Figures S3, S4 and S5)

**Figure 4.**

(A) Pie charts of the most abundant sgRNAs in three individual lobes of the lungs of two representative mice transplanted with mGeCKOa transduced cells. The area for each sgRNA corresponds to the fraction of total reads from the lobe for the sgRNA. All sgRNAs with 2% of total reads are plotted individually.

(B) Pie charts of the most abundant sgRNAs in the lung (averaged across three individual lobes) for the two mice shown in (A). All sgRNAs with 2% of average reads are plotted individually.

- (C) *Left*: Percentage of late tumor reads for the significantly enriched (FDR < 0.2%) mGeCKOa sgRNAs found in the lung metastases (averaged across three dissected lobes). *Right*: In purple, the percentage of late tumor reads for the significantly enriched (FDR < 0.2%) mGeCKOa sgRNAs found in the lung metastases (average across all mice, $n = 9$ mice). In grey, the percentage of late tumor reads for random, size-matched samplings of sgRNAs present in the late tumor ($n = 100$ samplings).
- (D) *Inset*: All sgRNAs found in individual lung lobes ordered by the percent of lobes in which a particular sgRNA was amongst the significantly enriched (FDR < 0.2%) sgRNAs for that lobe. Only sgRNAs enriched in 2 or more lobes are shown. *Main panel*: Enlargement and gene labels for sgRNAs at the top of the list from the inset (boxed region).
- (E) *Inset*: All sgRNAs found in individual mouse (averaged across three dissected lobes) ordered by the percent of mice in which a particular sgRNA was amongst the significantly enriched (FDR < 0.2%) sgRNAs for that mouse. Only sgRNAs enriched in 2 or more mice are shown. *Main panel*: Enlargement and gene labels for sgRNAs at the top of the list from the inset (boxed region).
- (F) *Bottom*: Metastasis Primary Ratio (MPR) for the sgRNAs in mGeCKOa with enrichment in metastases over late tumor (MPR > 1) observed in at least 3 mice. The sgRNAs are sorted by the number of mice in which the MPR for the sgRNA is greater than 1. *Top*: Number of mice in which the MPR for this sgRNA is greater than 1. In both panels, individual sgRNAs are labeled by gene target.
- (G) Number of genes with 0, 1, 2 or 3 significantly enriched (FDR < 0.2% for at least one mouse) mGeCKOa sgRNAs in the lung metastases. For genes with 2 enriched sgRNAs, gene names are indicated in the colored bubble adjacent to the bar.
- (H) Number of mice and percentage of mice in which each sgRNA was enriched in the lung metastases for all genes with multiple enriched sgRNAs.
- (See also: Figures S4 and S5)

**Figure 5.**

(A) Schematic representation of lentiviral transduction of Cas9-GFP KPD cells with single sgRNAs designed to target one gene or miRNA. After puromycin selection, the cell population was transplanted into *Nu/Nu* mice and also deep sequenced to examine the distribution of indels at the target site. After 5 weeks, the primary tumor and lungs are examined.

(B) Histograms of indel sizes at the genomic locus targeted by a representative sgRNA for each gene/miR after 3 days of puromycin selection. Indels from sgRNAs targeting the same gene were pooled (6 sgRNAs for each protein-coding gene, 4 sgRNAs for each miR).

(C) Representative H&E staining of lung lobes from uninjected mice ($n = 3$ mice), mice transplanted with cells transduced with Cas9 only ($n = 5$), and mice transplanted with cells containing Cas9 and a single sgRNA ($n = 6$). Single sgRNAs are either control/non-targeting sgRNAs ($n = 6$ mice for control sgRNAs, 3 distinct control sgRNAs with 2 mice each) or targeting sgRNAs ($n = 6$ mice for each gene/miR target, 3 sgRNAs per target with 2 mice each). Blue arrows indicate lung metastases. Scale bar: 10 μm .

(D) Percent of lung lobes with metastases after 6 weeks for the mice in (C).

(E) Primary tumor growth curve of *Nu/Nu* mice transplanted with NSCLC cells transduced with Cas9 only ($n = 5$) or single sgRNAs ($n = 6$ mice per gene/miR target, 3 sgRNAs per target with 2 mice each; $n = 6$ mice for control sgRNAs, 3 control sgRNAs with 2 mice each).

(F) Correlation between primary tumor volume and percent of lobes with metastases for each gene in (D) and (E). Error bars indicate *s.e.m.*.

(See also: Figure S6)

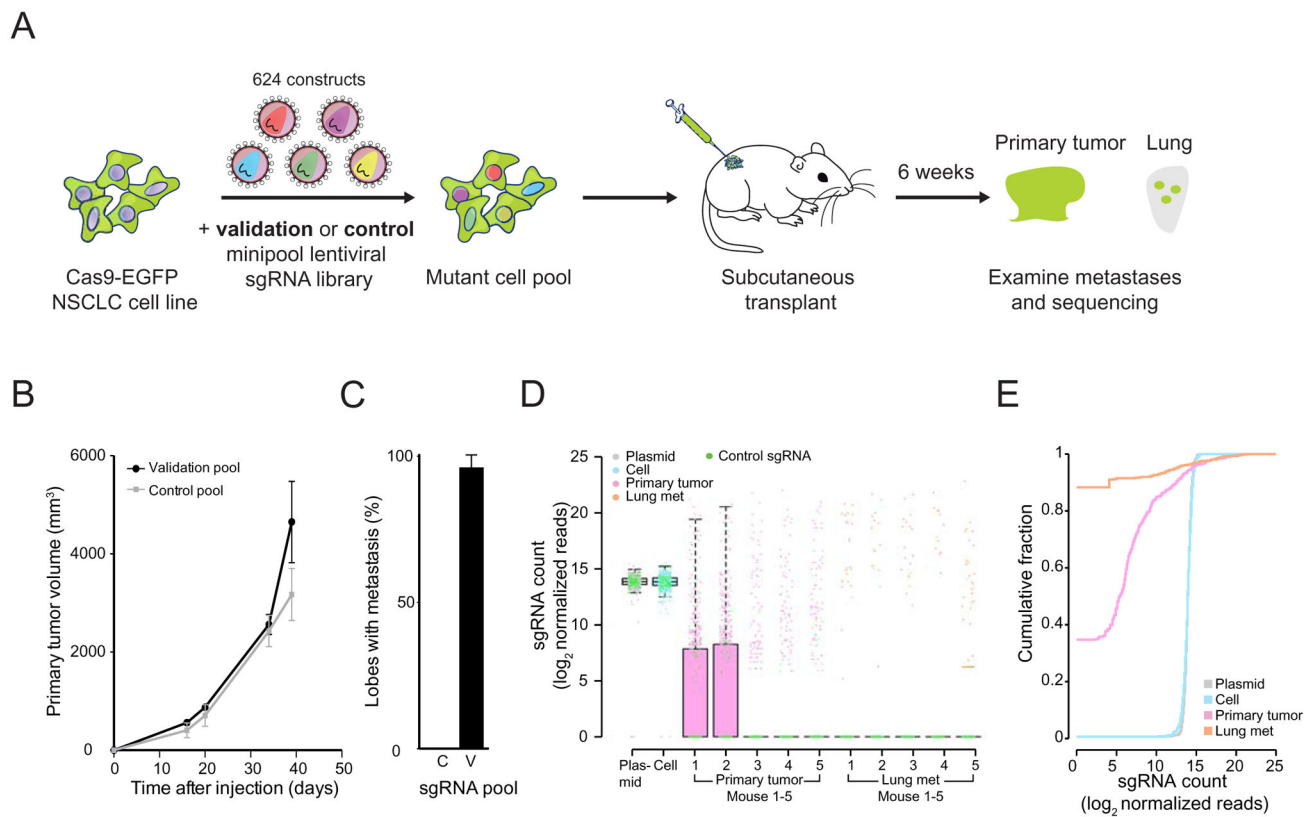


Figure 6.

(A) Schematic representation of the loss-of-function metastasis minipool screen. Briefly, Cas9-GFP KPD cells were transduced with either validation minipool (524 gene-targeting + 100 non-targeting sgRNAs) or control minipool (624 non-targeting sgRNAs). After puromycin selection, the cell pools are transplanted into *Nu/Nu* mice. After 6 weeks, validation minipool sgRNAs are sequenced from primary tumor and lung samples.

(B) Primary tumor growth curve of *Nu/Nu* mice transplanted with Cas9 vector + validation minipool cells ($n = 5$ mice) or Cas9 + control minipool cells ($n = 5$ mice).

(C) Percent of lung lobes with metastases after 6 weeks for the mice in (B). C = control minipool. V = validation minipool.

(D) Boxplot of the sgRNA normalized read counts for the plasmid library, cells before transplantation, primary tumor and lung metastases using the validation minipool.

(E) Cumulative probability distribution of library sgRNAs in the validation plasmid pool, cells before transplantation, early tumor and lung metastases. Distributions of primary tumor and lung metastases are averaged across 5 mice.

(See also: Figure S7)

categorized by how many sgRNAs targeting that gene/miRs are enriched as indicated in the colored bubbles adjacent to each bar.

(E) Schematic illustration of tumor growth and metastasis in the library-transduced NSCLC transplant model. The initially diverse set of loss-of-function mutations in the subcutaneously transplanted pool is selected over time for mutations that promote growth of the primary tumor. A subset of these mutants also dominate lung metastases.

(See also: Figure S7)